VII International Conference on Computational Methods in Marine Engineering
MARINE 2017
M. Visonneau, P. Queutey and D. Le Touzé (Eds)

TOWARDS THE HIGH-FIDELITY MULTIDISCIPLINARY DESIGN OPTIMIZATION OF A 3D COMPOSITE MATERIAL HYDROFOIL

SILVIA VOLPI[*], MATTEO DIEZ[†*] AND FREDERICK STERN[*]

[*]IIHR-Hydroscience and Engineering, The University of Iowa
100 C. Maxwell Stanley Hydraulics Laboratory, Iowa City, IA 52242, USA
e-mail: frederick-stern@uiowa.edu

[†]CNR-INSEAN, National Research Council-Marine Technology Research Institute
Via di Vallerano 139, 00128 Rome, Italy

Key words: Multidisciplinary design optimization, Fluid-structure interaction, Design space dimensionality reduction, Surrogate models, Adaptive sampling

Abstract. The development of a multidisciplinary design optimization (MDO) architecture for high-fidelity fluid-structure interaction (FSI) problems is presented with preliminary application to a NACA 0009 3D hydrofoil in metal and carbon-fiber reinforced plastic materials. The MDO methodology and FSI benchmark solution are presented and discussed. The computational cost of the MDO is reduced by performing a design space dimensionality reduction beforehand and integrating into the architecture a variable level of coupling between disciplines, a surrogate model, and an adaptive sampling technique. The optimization is performed using a heuristic global derivative-free algorithm. The MDO method is demonstrated by application to an analytical test problem. Current stage of research includes preliminary test problem optimization, validation of the hydrofoil FSI against experimental data, and design space assessment and dimensionality reduction for the hydrofoil model.

1 INTRODUCTION

The design of water-borne vehicles and components relies on high-fidelity simulations, organized to provide the performance of alternative designs in a variety of operating and environmental conditions. The simulation-based design (SBD) approach generally includes a hydrodynamic and/or structural solver, a design modification tool, and optimization algorithms and has been successfully applied to deterministic and stochastic optimization of a variety of ships. Lately, [2] successfully applied SBD methods based on RANS to the deterministic optimization of a fast catamaran in calm water. Extensions to stochastic SBD for ships in realistic ocean conditions were presented in [3] and applied to the same catamaran model. Both deterministic and stochastic optimization methods relied solely on a high-fidelity hydrodynamic solver and did not account for the elastic structural response of the ship.

Fluid-structure interaction (FSI) may be of paramount significance in specific phenomena, such as slamming, springing, and whipping of ships, as well as hydro-elastic effects of rudders, propellers, and appendages in general. To predict accurately the effects of FSI on the hydro-structural performance in SBD, high-fidelity FSI solvers are required along with their validation in complex realistic conditions. Recent research by the authors showed the full-scale validation of a partitioned FSI solver based on one- and two-way URANS/FE coupling for a high-speed craft with composite panels, slamming in waves [16]. The effects of FSI were found significant,

motivating further FSI methodology development and the integration of FSI into the SBD via multidisciplinary design optimization (MDO).

MDO refers to optimization procedures where the design performance depends on several interconnected disciplines. MDO architectures define the coupling between disciplines (such as strong or weak) and the sequence of tasks required to achieve both the multidisciplinary consistency and the solution of the design optimization problem. In the context of FSI, the availability of experimental data is essential to validate the multidisciplinary consistency achieved by the process. Lately, FSI data [17] of a NACA 0009 3D hydrofoil have been used as a benchmark for numerical hydrodynamic [8], FSI and MDO studies, investigating the effects of multiple materials (metals and composite).

High-fidelity MDO of complex engineering problems represents a technological challenge. Complexity of the multidisciplinary analysis and an often-large number of design variables are critical factors affecting the computational cost. Design space dimensionality reduction techniques and surrogate models can be used to alleviate the computational resource consumption. Design space dimensionality reduction is generally performed by sensitivity analysis, requiring fully-coupled multidisciplinary analyses and not addressing the interdependence of design variables. To overcome these limitations, an offline design space dimensionality reduction method for shape optimization has been recently presented [4],[5] based on the Karhunen-Loève expansion (KLE) of the shape modification vector. The technique adopts a purely geometrical perspective and precedes any analysis/optimization process. Surrogate models have been extensively used in several engineering fields. Examples of multidisciplinary applications are given in [13] and [14]. The combination of surrogate models and adaptive sampling techniques has been investigated in earlier research [18],[15] showing promising improvements in accuracy and efficiency.

The objective of the current research is the development of an MDO architecture for high-fidelity optimization of complex FSI problems, with application to a NACA 0009 3D hydrofoil in carbon fiber-reinforced plastic (CFRP). The MDO methodology and FSI benchmark solution are presented and discussed.

Specifically, the design space dimensionality reduction is performed beforehand by extension of the combined distributed/concentrated parameters KLE presented in [6] to purely geometrical quantities. The identification of the optimal design is achieved by sequential surrogate-based global derivative-free optimization using dynamic radial basis functions (DRBF) [15] and deterministic particle swarm optimization (DPSO) [1]. The multi-criterion adaptive sampling (MCAS) [7] is extended to multi-disciplinary optimization allowing for a variable level of coupling between fluid and structural dynamics. As the analysis advances, the design space is explored and the multidisciplinary consistency refined. A steady two-way coupled FSI is solved using Gauss-Seidl iterations. Current status of the research includes: (a) a preliminary analytical test problem optimization (including comparison of the current architecture to a standard multidisciplinary feasible, MDF [10], approach), (b) the validation of FSI analysis against experimental data for the hydrofoil in stainless steel, aluminum, and CFRP, and (c) design space assessment and dimensionality reduction.

2 PROBLEM STATEMENT AND NUMERICAL METHODS

2.1 Multidisciplinary design optimization: statement of the problem and architecture

The multidisciplinary design optimization problem for FSI is formulated as follows

$$\min_{\mathbf{u}} f[\mathbf{u}, \mathbf{y}(\mathbf{u}, \mathbf{y})] \tag{1}$$

$$\begin{aligned} \text{subject to } & \mathbf{c}_0[\mathbf{u}, \mathbf{y}(\mathbf{u}, \mathbf{y})] \leq 0 \\ & \mathbf{c}_F[\mathbf{u}_0, \mathbf{u}_F, \mathbf{y}_F(\mathbf{u}_0, \mathbf{u}_F, \mathbf{y}_S)] \leq 0 \\ & \mathbf{c}_S[\mathbf{u}_0, \mathbf{u}_S, \mathbf{y}_S(\mathbf{u}_0, \mathbf{u}_S, \mathbf{y}_F)] \leq 0 \end{aligned}$$

where f is the objective function, $\mathbf{c}$ is the set of constraint functions, $\mathbf{u}$ is the set of design variables, and $\mathbf{y}$ is the set of coupling variables from fluid and structural analyses. Design variable bounds are handled directly by the optimizer. The subscript $(\cdot)_F$ indicates the fluid analysis, $(\cdot)_S$ refers to the structural analysis, and $(\cdot)_0$ indicates that the variable/function is shared by both disciplines. The inequality constraints $\mathbf{c}$ are handled by a linear penalty function. This allows for recasting the formulation in Eq. 1 into the following unconstrained optimization

$$\min_{\mathbf{u}} f_p[\mathbf{u}, \mathbf{y}(\mathbf{u}, \mathbf{y})] \tag{2}$$

where f_p is the penalized objective function defined as

$$f_p = f + \gamma \sum_{i=1}^{N_{c0}} \max\{\mathbf{c}_0, 0\} + \gamma \sum_{i=1}^{N_{cF}} \max\{\mathbf{c}_F, 0\} + \gamma \sum_{i=1}^{N_{cS}} \max\{\mathbf{c}_S, 0\} \tag{3}$$

and γ is a penalty coefficient.

The optimization is solved using sequential surrogate models trained by objective function values provided by the FSI analysis. The density of the training points is improved by infill of new samples at each iteration. The FSI coupling is initially loose and gets tighter as the optimization advances. The procedure is shown in the block diagram of Figure 1.

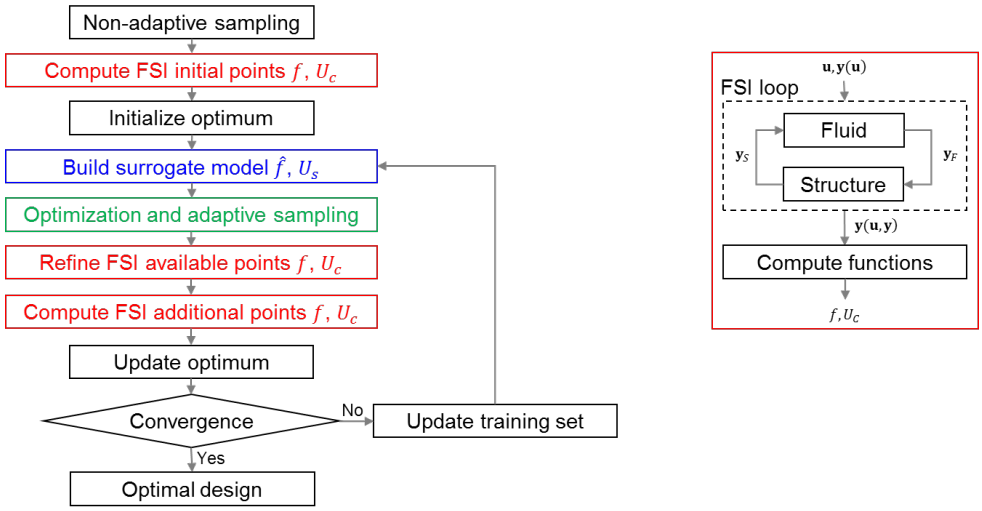

Figure 1: MDO solution procedure and FSI loop

The DRBF surrogate model provides the prediction of the function $\hat{f}(\mathbf{u})$ as the expected value of a sample of standard RBF predictions over a stochastic distribution of a tuning parameter associated with the RBF kernel. The sampling uncertainty $U_s(\mathbf{u})$ is the 95% confidence interval of the stochastic sample. Details of the method can be found in [15]. The FSI loop is driven by Gauss-Seidl iterations between the fluid and the structural solvers. A coupling uncertainty U_C is defined based on the convergence of the Gauss-Seidl loop and quantified by the difference between two consecutive iterations.

The adaptive sampling technique MCAS identifies groups of new samples for training the DRBF model aiming at balancing the surrogate model accuracy and the search for the global

minimizer. In case of single-discipline optimization, this is performed by solving the multi-objective optimization problem

$$\min_{\mathbf{u}} \hat{f}_p(\mathbf{u}) \text{ and } \max_{\mathbf{u}} U(\mathbf{u}) \tag{4}$$

where U is the uncertainty of the surrogate model U_s, depicted in Figure 2a. The resulting Pareto front is down-sampled to identify I equally spaced points along the curve as shown in Figure 2b. Details of the method are provided in [7].

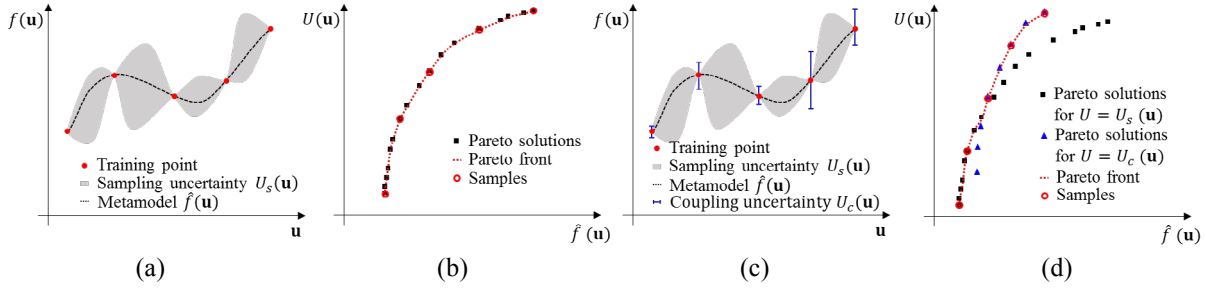

(a) (b) (c) (d)

Figure 2: Single-discipline (a, b) and multidisciplinary (c, d) MCAS

In case of multidisciplinary optimization, MCAS accounts for both $U_s(\mathbf{u})$ and $U_c(\mathbf{u})$. As shown in Figure 2c, U_s is continuous and goes to zero at the training points; U_c is instead discrete and defined only at the training points. Two independent Pareto sets, $\wp_s$ and $\wp_c$, are built using $U = U_s$ and $U = U_c$ in Eq. 4 and are depicted in Figure 2d. A new set $\wp$ is defined taking the non-dominated solutions of $\wp_s \cup \wp_c$, with the additional constraints, $U > U_{min}$ (in order to avoid overshooting in training the surrogate model) and $\hat{f} - \hat{f}^* > U_{tot}$ where $U_{tot} = \sqrt{U^2 + U^{*2}}$ (* indicates current optimum values). $\wp$ is down-sampled as in the standard MCAS. If a sample is determined that was originally in $\wp_c$ the corresponding function value in the training set is updated by refining the FSI analysis. If a sample is determined that was originally in $\wp_s$ a new point is added to the training set. The method is referred to as MCAS with concurrent uncertainties (MCAS-CU). The multi-objective version [11] of the DPSO algorithm is applied to solve Eq. 4 and extract the Pareto sets.

2.2 Fluid-structure interaction

The fluid is modeled by the continuity and RANS equations for incompressible Newtonian viscous flow. The CFD finite difference code CFDShip-Iowa V4.5 [9] is used to solve continuity and momentum equations along with the turbulence equations for the Menter's blended k-ω/k-ε model. The structural equation of elastic motion is solved by a modal expansion, where modes and frequencies are provided by the computational structural dynamics (CSD) solver ANSYS Mechanical APDL V15, a commercial FE code.

In the Gauss-Seidl iterations for steady FSI, $\mathbf{y}_F$ and $\mathbf{y}_S$ are the hydrodynamic load predicted by the fluid solver and the displacement predicted by the structural solver, respectively, at the fluid-structure interface. The hydrodynamic load is transferred from the fluid to the structure mesh by Gauss interpolation of the force distribution $\mathbf{f}(\mathbf{x})$ so that $\mathbf{f}_F(\mathbf{x}) \approx \mathbf{f}_S(\mathbf{x})$ and $\mathbf{F}_F \approx \mathbf{F}_S$, where $\mathbf{F} = \int \mathbf{f}(\mathbf{x}) d\mathbf{x}$ is the total force. The current interpolation approach allows for force conservation, while moments are conserved only in an asymptotic sense, i.e. for a mesh size that goes to zero. When transferring the displacement from the structure to the fluid mesh, the deformation is interpolated in the entire volume representing the fluid domain. The fluid volume mesh is structured with indices I, J, and K, where $J = 1$ corresponds to the fluid-solid interface.

First, the $J = 1$ surface is deformed by Gauss interpolation so that $\boldsymbol{\delta}_S(\mathbf{x}) \approx \boldsymbol{\delta}_F(\mathbf{x})$. Then, the volume inner nodes are displaced by linear interpolation between interface ($J = 1$) and outer ($J = J_{MAX}$) boundary layer surfaces. Details and applications of the FSI routine are given in [16].

2.3 Shape modification, design-space assessment and dimensionality reduction

The shape modification is performed using free-form deformation (FFD) [12]. The method allows for smooth deformations of an arbitrary object by deformation of the 3D space embedding the object. The deformation is propagated in the space from displacement of discrete control points. The design variables are the displacements of the control points.

The design space assessment and dimensionality reduction are performed considering the breakdown of the geometric variance associated to the shape modification space. The method is based on the KLE of the shape modification vector [4]. It is extended here to a combined distributed/concentrated geometrical parameter vector, similarly to what introduced in [6] to integrate physical parameters in the design space assessment.

The aim of the KLE is to find an optimal basis of orthonormal functions for the linear representation of the shape modification $\widehat{\boldsymbol{\gamma}}(\mathbf{x},\mathbf{u}) = \sum_{k=1}^{\infty} \alpha_k(\mathbf{u})\boldsymbol{\psi}_k(\mathbf{x})$, where

$$\widehat{\boldsymbol{\gamma}}(\mathbf{x},\mathbf{u}) = \begin{cases} \widehat{\boldsymbol{\delta}}(\mathbf{x},\mathbf{u}), \mathbf{x} \in D \\ \widehat{\boldsymbol{\theta}}(\mathbf{x},\mathbf{u}), \mathbf{x} \in C \end{cases} \quad \text{and} \quad \boldsymbol{\psi}_k(\mathbf{x}) = \begin{cases} \boldsymbol{\varphi}_k(\mathbf{x}), \mathbf{x} \in D \\ \boldsymbol{\upsilon}_k(\mathbf{x}), \mathbf{x} \in C \end{cases} \tag{5}$$

with D and C being the domains of the distributed and concentrated modifications $\widehat{\boldsymbol{\delta}}$ and $\widehat{\boldsymbol{\theta}}$, respectively. In the present work, $\widehat{\boldsymbol{\delta}}$ is the distributed shape modification vector (displacement) and $\widehat{\boldsymbol{\theta}}$ includes twist and camber at specified sections. The basis retaining the maximum variance is determined by solution of an eigenvalue problem [4]. The KLE eigenvalues λ_k represent the design variability (variance) associated to the corresponding KLE modes $\boldsymbol{\psi}_k$. Provided that $\lambda_k \geq \lambda_{k+1}$, the reduced-dimensionality design space is built by truncating the linear expansion to the order N, so as to resolve a desired level of geometric variability $\sum_{k=1}^{N} \lambda_k$. The coefficients α_k are used as new design variables of the reduced-dimensionality design space.

3 ANALYTICAL TEST CASE

The MDO architecture is applied to the following two-dimensional test problem:

$$\begin{aligned} \min_{\mathbf{u}} \quad & f(\mathbf{u}) = u_1^2 + u_2 + y_1 + e^{-y_2} \\ \text{with} \quad & y_1(\mathbf{u}, y_2) = 100 + u_1 + u_2 - 0.2y_2 \\ & y_2(\mathbf{u}, y_1) = \sqrt{|y_1|} + 10 + u_2 \end{aligned} \tag{6}$$

Box-constraints are $-10 \leq u_1 \leq 25$ and $-25 \leq u_2 \leq 10$. The problem is solved using a convergence criterion based on the coupling uncertainty U_c in the neighborhood of the optimum. U_c and U_{min} are set equal to 10^{-4}. The RBF kernel used is a power law with exponent uniformly distributed between 1 and 3. Results are compared with the standard MDF architecture. The latter applies single-objective DPSO directly to objective function evaluations reaching multidisciplinary consistency (with tolerance 10^{-4}). Both methods are initialized by a Hammersley sequence distribution of 16 points. Single- and multi-objective DPSO uses 16 particles for 100 iterations.

The convergence of the optimum is depicted in Figure 3a including the optimal solution as predicted by the surrogate model $\hat{f}_s$, the total uncertainty in prediction U_{tot}, and the true value of f. In approximately 4 iterations U_{tot} reduces significantly (0.01%) and the surrogate model

prediction appears accurate. A breakdown of the uncertainty is provided in Figure 3b showing U_s and U_c. The current architecture outperforms a standard MDF with equivalent tolerance for U_c, as shown by Figure 3c. The number of function evaluations needed to achieve the optimum is smaller by an order of magnitude. The distribution of samples for the two architectures is shown in Figure 4.

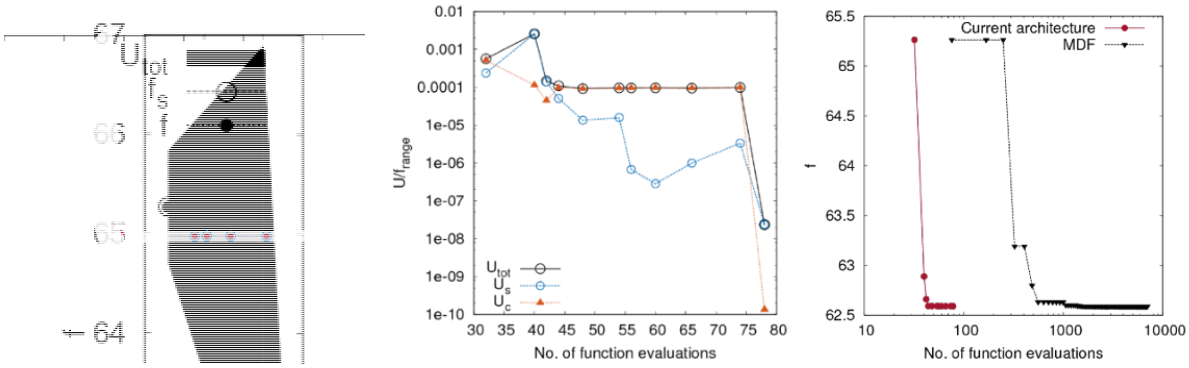

(a) (b) (c)

Figure 3: Convergence of (a) optimum, (b) uncertainties, and (c) comparison with MDF

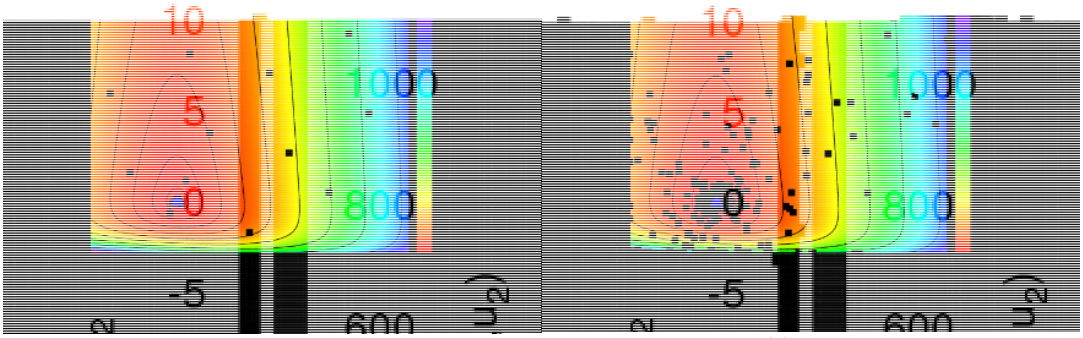

(a) Current architecture (a) MDF

Figure 4: Current architecture sampling

4 INDUSTRIAL TEST CASE

The 3D hydrofoil (Figure 5 and Table 1) is tapered with streamlined NACA 0009 cross-sections and is clamped at the root section. An experimental study was carried out at the University of Tasmania-AMC to investigate the steady hydro-elastic behavior of the hydrofoil comparing different materials, including stainless steel, aluminum, and two sandwich structures manufactured with CFRP external skins and inner foam core [17]. The CFRP hydrofoils differ in fiber orientation: CFRP00 fibers are aligned with the span whereas CFRP30 fibers are at a 30 degrees angle. The models have thicker trailing edge then standard NACA 0009 to accommodate the composite material. Lift C_L, drag C_D, and pitching moment C_M coefficients, tip displacement δ and twist θ are available from water tunnel testing for several Reynolds number and angles of attack.

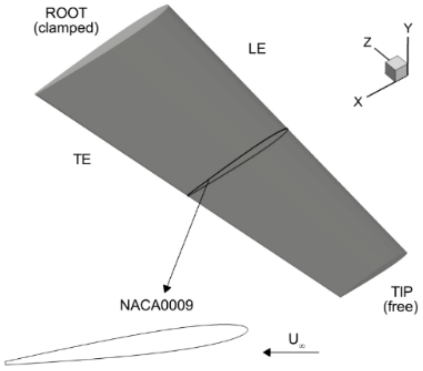

Figure 5: 3D hydrofoil geometry

Table 1: 3D hydrofoil parameters

Chord length at root	0.12 m
Chord length at tip	0.06 m
Mean chord length	0.09 m
Span length	0.3 m
Aspect ratio	3.33
Cross-section	NACA0009

4.1 Fluid-structure interaction

Steady two-way coupling FSI is performed at an angle of attack (α) equal to 8 degrees and a Reynolds number equal to 0.6×10^6. The condition is in the pre-stall range providing steady hydrodynamics. The two-way FSI analysis focuses on the validation of C_L, C_D, C_M, δ, and θ.

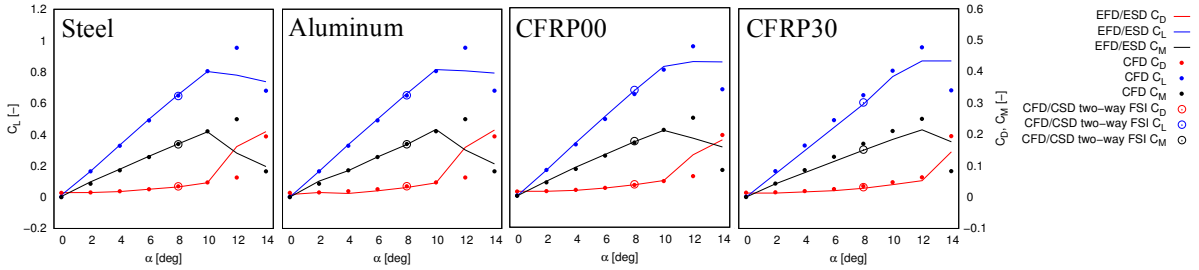

Figure 6: Lift, drag, pitching moment coefficients

Figure 6 show the C_L, C_D, and C_M curves including CFD simulations, FSI simulations, and experimental data (EFD/ESD). The deformation of steel and aluminum hydrofoils is small, affecting only slightly the hydrodynamic forces. Both CFD simulations for rigid body and FSI simulations provide a good approximation of the curves. At α = 8 degrees, the errors for C_L, C_D, and C_M between FSI and experiments (as percentage of the experimental dynamic range) are -1.11, 0.97, and -0.72% for steel and -1.43, 2.01, and -0.11% for aluminum.

The deformation of the CFRP00 hydrofoil is larger than the metals and for the CFRP30 is particularly significant, leading to a visible discrepancy between experimental and CFD curves (with errors up to 10%). The errors between FSI and experiments are smaller and equal 0.46, 1.03, and 1.11% for CFRP00 and 1.77, 2.00, and 1.05% for CFRP30 for C_L, C_D, and C_M, respectively. Overall, the FSI prediction of hydrodynamic forces is found accurate with a maximum error close to 2%.

The hydrodynamic efficiency C_L/C_D is shown in Figure 7. The experimental values for steel, aluminum, CFRP00, and CFRP30 are 20.1, 21.4, 19.3, and 21.3. Those computed by FSI are 18.7, 18.7, 18.3, and 19.1. The experimental data for aluminum shows large peaks between 4 and 8 degrees, which appear likely to be outliers. Excluding those, CFRP30 provides the largest efficiency overall.

Figure 8 shows the hydrofoil shape computed by the FSI focusing on the tip deformation. The tip displacement for steel and aluminum is small (less than 3% of span) and the twist is

negligible. The error between FSI and experiments for steel and aluminum is -7.6 and -18% of the experimental pre-stall range. The tip displacement for CFRP00 is approximately 3% of the span whereas it is 6% of span for CFRP30. 0.5 degrees positive tip twist is found for CFRP00 and 1.5 degrees of negative twist for CFRP30. The errors for CFRP00 and CFRP30 are -6.2 and -13% for δ and 36% and 1.2% for θ, respectively. Overall, δ is under-predicted by the FSI but the trend is captured.

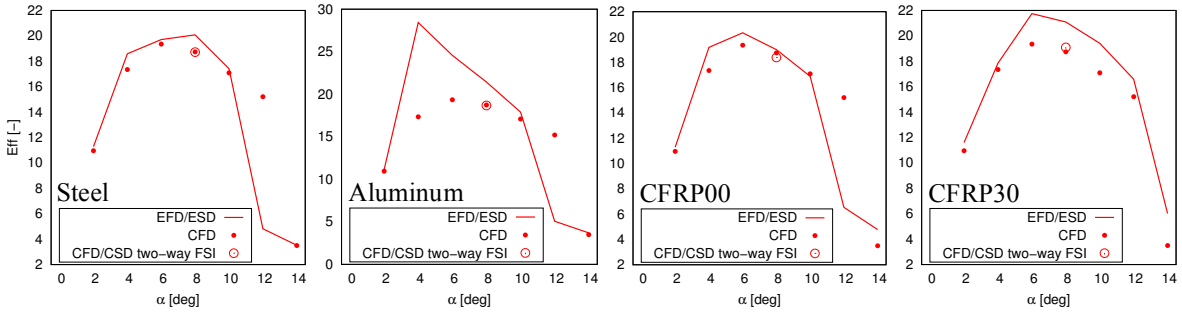

Figure 7: Hydrodynamic efficiency

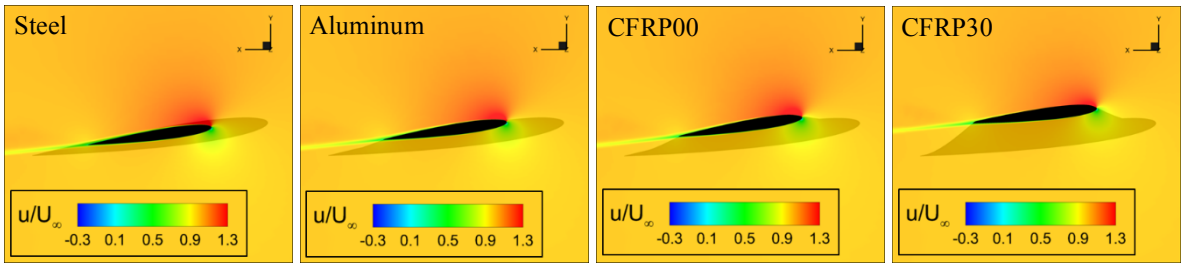

Figure 8: Deformation and contour of the x-velocity at 95% of the span

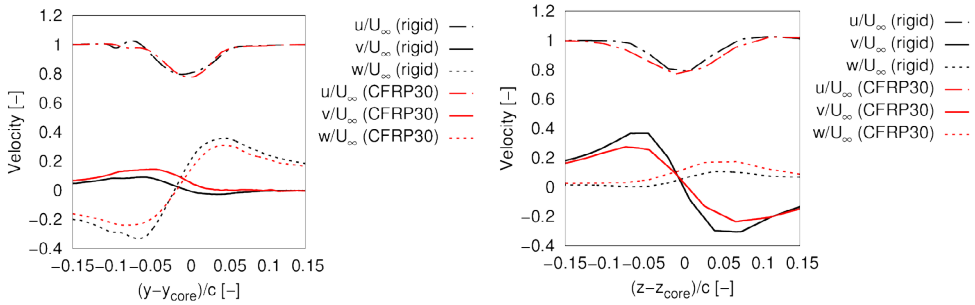

Figure 9: Velocity distribution along y and z axes at the vortex core

CFRP30 results for θ are consistent with the experimental hydrodynamic curves, showing a reduction of forces and moment compared to the CFD. The stall-delay effect is due to the negative twist of the tip section, which reduces the effective angle of attack. The associated efficiency increase is due to the reduction of tip vortex intensity. Figure 9 depicts the non-dimensional velocity distributions through the vortex core comparing CFRP30 with the rigid hydrofoil. The CFRP30 shows a smaller fluctuation in the predominant velocity component. Moreover, at the tip vortex core and downstream the tip trailing edge (x = 0.06m), the second invariant of the rate of strain tensor Q, taken as criterion for vortex identification, is equal to 11600 for rigid body and 5500 for CFRP30. Overall, the FSI simulation captures the behavior of the structure giving a realistic description of the physics involved.

4.2 Shape modification and design space assessment

Four distributions of FFD control points are compared, as shown in Figure 10. Control points are allowed to move in the chord- (x) and thickness-wise (y) directions, whereas their position along the span (z) is fixed. Table 2 summarizes the FFD setups including the number of associated design variables. Additional design variables are included in the geometry modification. Rigid displacement and rotation of the sections are imposed. Bounds for all x/y displacements are set equal to $\pm$20% of the mean chord; bounds for the rotations are set equal to $\pm$15 degrees. Overall, five design spaces are analyzed and summarized in Table 3. DS1 to 4 have no rigid section displacement and uses a linear distribution for section rotation. DS5 includes independent rigid displacements and rotations at 5 sections.

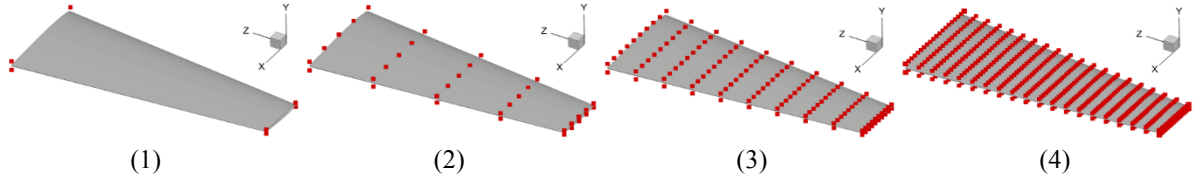

(1) (2) (3) (4)

Figure 10: FFD control points distribution

Table 2: FFD setups

Setup	Control points distribution	Number of variables
1	2x2x2	16
2	5x2x5	100
3	10x2x10	400
4	20x2x20	1600

Table 3: Design space parameters and variance

Design space	FFD setup	Additional DOF	Total number of design variables
DS1	1	1	17
DS2	2	1	101
DS3	3	1	401
DS4	4	1	1601
DS5	2	12	112

Table 4 gives the geometric variance σ^2 of the five design spaces computed using a standard KLE method. The comparison of DS1 to 4 shows that increasing the number of control points in the FFD reduces σ^2. The comparison of DS2 and DS5, which share the same FFD setup, shows that using additional rigid displacements and rotations increases σ^2. Overall, DS5 has the largest σ^2. Figure 11 displays the KLE eigenvalues convergence. The number of eigenvalues required to retain the 50, 75, 90, 95, 99, and 99.9% of σ^2 is summarized in Table 4 and labeled in Figure 11.

Table 4: Design space variance assessment

Design space	σ^2	No. of modes for X% of σ^2					
		50	75	90	95	99	99.9
DS1	$4.34\text{x}10^{-6}$	3	7	10	12	14	16
DS2	$1.42\text{x}10^{-6}$	8	16	27	36	54	77
DS3	$6.90\text{x}10^{-7}$	16	32	55	73	116	175
DS4	$3.50\text{x}10^{-7}$	27	59	105	141	226	347
DS5	$4.61\text{x}10^{-6}$	3	5	11	19	38	63

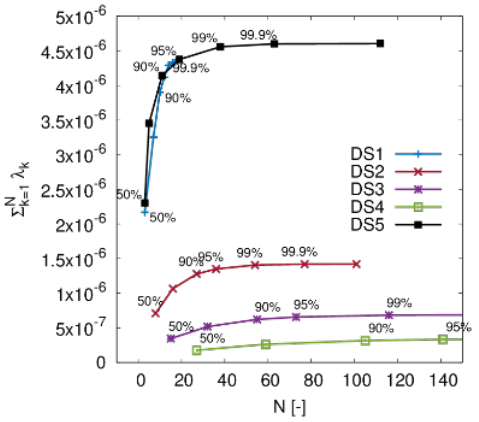

Figure 11: Eigenvalues convergence

Table 5: Combined distributed/concentrated geometric parameters for KLE analysis

Displacement weight	Twist weight	Camber weight	No. of modes for X% of σ^2					
			50	75	90	95	99	99.9
1.0	0.0	0.0	3	5	11	19	38	63
0.9	0.05	0.05	3	6	13	20	39	65
0.8	0.1	0.1	4	6	12	19	38	64
0.6	0.2	0.2	4	6	11	17	35	61
0.5	0.25	0.25	3	6	10	15	33	59
0.333	0.333	0.333	2	5	9	12	28	54

When performing combined distributed/concentrated parameter KLE, a weight is assigned to distributed (displacements) and concentrated (twist and camber) modifications. DS5 is evaluated comparing six sets of relative weights. The number of eigenvalues required to retain the 50, 75, 90, 95, 99, and 99.9% of σ^2 is summarized in Table 5. Using even weights for the three parameters provides the most efficient dimensionality reduction.

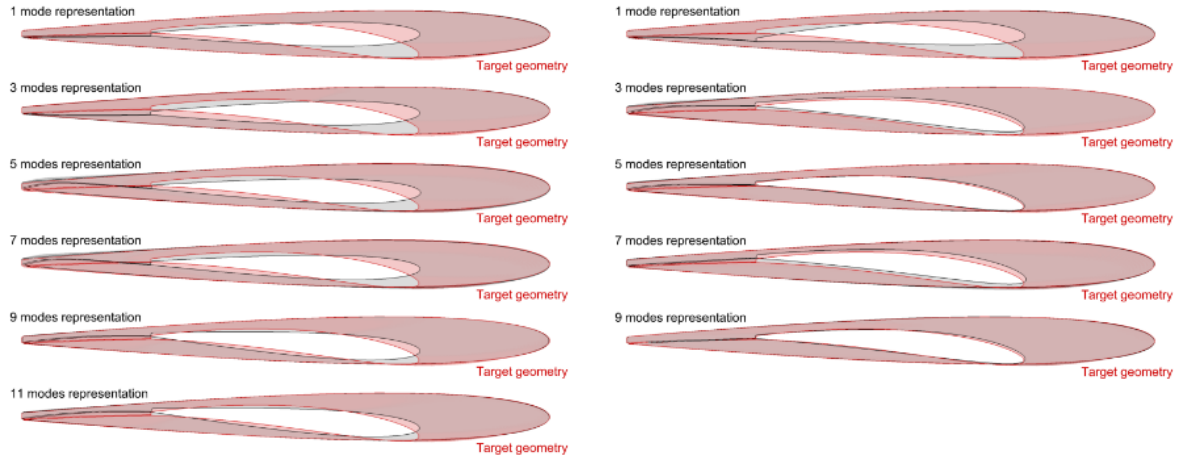

(a) Distributed parameter KLE

(b) Combined distributed/concentrated parameter KLE

Figure 12: Target geometry representation

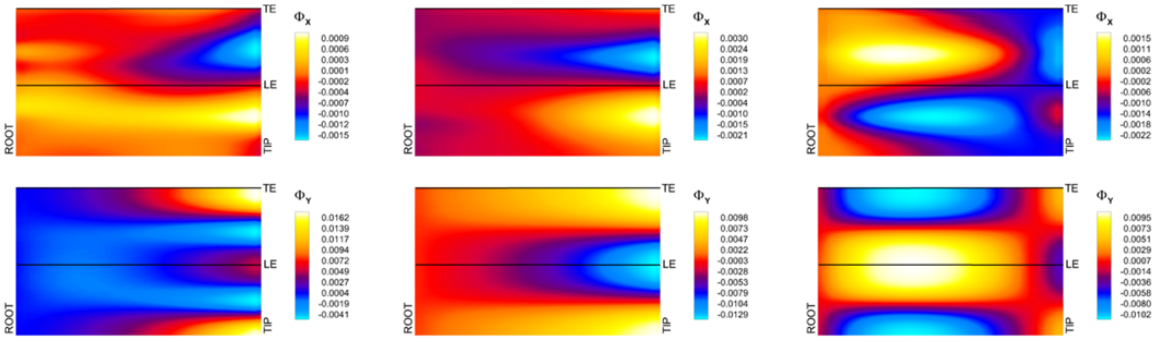

(1) (2) (3)

Figure 13: Eigenvectors of DS5 representation with combined distributed/concentrated parameter KLE

A nearly optimal shape inspired by [8] is used as a target to test the accuracy of the reduced-dimensionality representation of the shape modification. Figure 12 shows the geometry reconstruction using a finite number of KLE modes comparing standard (a) and combined distributed/concentrated parameter KLE (b). The design space representation through the latter

method outperforms standard KLE in representing the target geometry. The first three eigenvectors used by the combined distributed/concentrated parameter KLE for representing DS5 are depicted in Figure 13.

4.3 Multidisciplinary design optimization

Ongoing MDO studies aim at the design optimization of the hydrofoil for maximizing the hydrodynamic efficiency at specified conditions. The multiple design choices offered by the CFRP material are investigated and a combined shape and structural design optimization is sought after.

9 CONCLUSIONS AND FUTURE RESEARCH

The development of an MDO architecture for high-fidelity FSI problems has been shown with preliminary application to a NACA 0009 3D hydrofoil in metal and CFRP materials. The MDO methodology and FSI benchmark solution were presented and discussed.

The methodology for high-fidelity MDO integrates design space dimensionality reduction, surrogate modeling, and adaptive sampling into a global derivative-free optimization framework. The architecture performs sequential surrogate-based optimization refining the accuracy of the analysis by infill of new samples and improvement of the multidisciplinary consistency. The MDO methodology was applied to a two-dimensional analytical test problem and compared with a standard MDF architecture employing the same optimization algorithm and convergence criterion. The current method outperforms the MDF requiring fewer function evaluations by an order of magnitude.

The FSI of the hydrofoil original geometry was studied and compared with available experimental data. The simulations showed an accurate description of the physics and prediction of lift and drag forces, pitching moment, hydrodynamic efficiency, tip displacement and twist. Results were shown for stainless steel, aluminum, and two types of carbon fiber-reinforced plastic (CFRP) materials. The negative tip twist provided by one of the CFRP materials correlates with lower tip vortex intensity, stall delay, and higher hydrodynamic efficiency.

Several design spaces for the hydrofoil were assessed by Karhunen–Loève expansion (KLE), showing geometric variability, convergence of the KLE eigenvalues, and capability in representing a target nearly optimal geometry. A novel KLE formulation based on combined distributed/concentrated geometrical parameters was used to build a more efficient reduced-order representation of the design space than standard KLE.

Future research includes the sensitivity analysis along KLE-provided design variables. The hydrodynamic shape optimization of the rigid hydrofoil will be performed along with the MDO of the aluminum and CFRP models.

ACKNOWLEDGEMENTS

The research is supported by the Office of Naval Research, grant N00014-14-1-0195 and NICOP grant N62909-15-1-2016, administered by Dr. Thomas Fu, Dr. Ki-Han Kim, and Dr. Woei-Min Lin. Matteo Diez is also grateful to the National Research Council of Italy for its support through the Short-Term Mobility Program 2015-2016.

REFERENCES

[1] E.F. Campana, G. Liuzzi, S. Lucidi, D. Peri, V. Piccialli, and A. Pinto, “New global optimization methods for ship design problems,” *Optimization and Engineering*, Vol. **10**, No. 4, pp. 533, (2009).

[2] X. Chen, M. Diez, M. Kandasamy, Z. Zhang, E.F. Campana, and F. Stern, "High-fidelity global optimization of shape design by dimensionality reduction, metamodels and deterministic particle swarm," *Engineering Optimization*, Vol. **47**, No. 4, pp.473–494, (2015).

[3] M. Diez, E.F. Campana, and F. Stern, "Development and evaluation of hull-form stochastic optimization methods for resistance and operability," *FAST 13th International Conference on Fast Sea Transportation*, Washington DC, USA, (2015).

[4] M. Diez, E.F. Campana, and F. Stern, "Design-space dimensionality reduction in shape optimization by Karhunen–Loève expansion," *Computer Methods in Applied Mechanics and Engineering*, Vol. **283**, pp. 1525–1544, (2015).

[5] M. Diez, A. Serani, E.F. Campana, S. Volpi, and F. Stern, "Design Space Dimensionality Reduction for Single- and Multi-Disciplinary Shape Optimization," *17th AIAA/ISSMO Multidisciplinary Analysis and Optimization Conference*, Washington, DC, USA, (2016).

[6] M. Diez, A. Serani, F. Stern, and E.F. Campana, "Combined geometry and physics based method for design-space dimensionality reduction in hydrodynamic shape optimization," *Proceedings of the 31st Symposium on Naval Hydrodynamics*, Monterey, CA, USA, (2016).

[7] M. Diez, S. Volpi, A. Serani, F. Stern, E.F. Campana, "Simulation-based design optimization by sequential multi-criterion adaptive sampling and dynamic radial basis functions," *EUROGEN International Conference on Evolutionary and Deterministic Methods for Design*, Glasgow, UK, (2015).

[8] N. Garg, G.K. Kenway, Z. Lyu, J.R. Martins, Y.L. Young, "High-fidelity hydrodynamic shape optimization of a 3-D hydrofoil," *Journal of Ship Research*, Vol. **59**, No. 4, pp. 209–26, (2015).

[9] J. Huang, P.M. Carrica, and F. Stern, "Semi-coupled air/water immersed boundary approach for curvilinear dynamic overset grids with application to ship hydrodynamics," *International Journal for Numerical Methods in Fluids*, Vol. **58**, No. 6, pp. 591–624, (2008).

[10] J.R. Martins and A.B. Lambe, "Multidisciplinary design optimization: a survey of architectures," *AIAA Journal*, Vol. **51**, No. 9, pp. 2049–2075, (2013).

[11] R. Pellegrini, E.F. Campana, M. Diez, A. Serani, F. Rinaldi, G. Fasano, U. Iemma, G. Liuzzi, S. Lucidi, and F. Stern, "Application of derivative-free multi-objective algorithms to reliability-based robust design optimization of a high-speed catamaran in real ocean environment," *Proceedings of the 4th International Conference on Engineering Optimization*, Lisbon, Portugal, (2014).

[12] T.W. Sederberg and S.R. Parry, "Free-form deformation of solid geometric models," *ACM SIGGRAPH computer graphics*, Vol. **20**, No. 4, pp.151–160, (1986).

[13] R.S. Sellar, S.M. Batill, and J.E. Renaud, "Response surface based, concurrent subspace optimization for multidisciplinary system design," *AIAA Journal*, Vol. **714**, (1996).

[14] J. Sobieszczanski-Sobieski and R.T. Haftka, "Multidisciplinary aerospace design optimization: survey of recent developments," *Structural Optimization*, Vol. **14**, No. 1, pp. 1–23, (1997).

[15] S. Volpi, M. Diez, N.J. Gaul, H. Song, U. Iemma, K.K. Choi, E.F. Campana, and F. Stern, "Development and validation of a dynamic metamodel based on stochastic radial basis functions and uncertainty quantification," *Structural and Multidisciplinary Optimization*, Vol. **51,** No. 2, pp. 347–368, (2015).

[16] S. Volpi, M. Diez, H. Sadat-Hosseini, D.-H. Kim, F. Stern, R.S. Thodal, J.L. Grenestedt, "Full-scale fluid-structure interaction simulation and experimental validation of high-speed planing-hull slamming with composite panels," *Proceedings of the 31st Symposium on Naval Hydrodynamics*, Monterey, CA, USA, (2016).

[17] G.A. Zarruk, P.A. Brandner, B.W. Pearce, and A.W. Phillips, "Experimental study of the steady fluid–structure interaction of flexible hydrofoils," *Journal of Fluids and Structures*, Vol. **51**, pp. 326–343, (2014).

[18] L. Zhao, K.K. Choi, and I. Lee, "Metamodeling method using dynamic kriging for design optimization," *AIAA Journal*, Vol. **49**, No. 9, pp. 2034–2046, (2010).